Aspect differences in vegetation type drive higher evapotranspiration on a pole-facing slope in a California oak savanna

Amanda Donaldson[1*], David Dralle[2], Nerissa Barling[1], Russell Callahan[1,3], Michael E. Loik[4], Margaret Zimmer[1,5]

[1]Department of Earth and Planetary Sciences, University of California, Santa Cruz, CA, USA.

[2]Pacific Southwest Research Station, United States Forest Service, Albany, CA, USA.

[3]Department of Earth Sciences, University of Connecticut, Storrs, CT, USA.

[4]Department of Environmental Studies, University of California, Santa Cruz, CA, USA.

[5]U.S. Geological Survey Upper Midwest Water Science Center, Madison, WI, USA.

Supplementary Information
Table of contents:
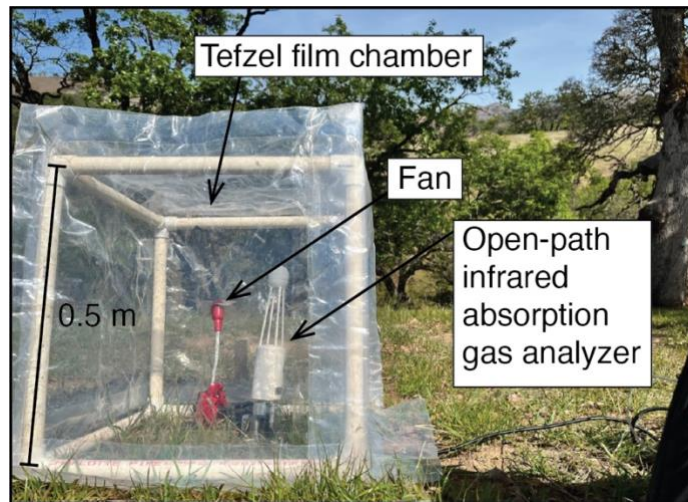
1.0 Supporting material methods

1.1. Grass transpiration methods

We measured water fluxes with an open-path, infrared gas analyzer (model LI-7500, LI-COR Inc., Lincoln, Nebraska) within a chamber (0.5 m x 0.5 m x 0.5 m) constructed of a PVC pipe frame and covered by Tefzel film with a fan placed inside to maximize chamber mixing (Supplementary Figure 1) (Huxman et al., 2004). We started data collection approximately 30 seconds after the chamber was secured flat on the ground surface to ensure no leakage from the chamber; each measurement lasted for approximately 90 seconds. We determined water fluxes by plotting the 1-second water flux accumulation measurements over the 90-second period. The slope of the change in concentration ($mg/m^3/s$) was converted into a flux ($mmols/m^2/s$) by using the following equation:
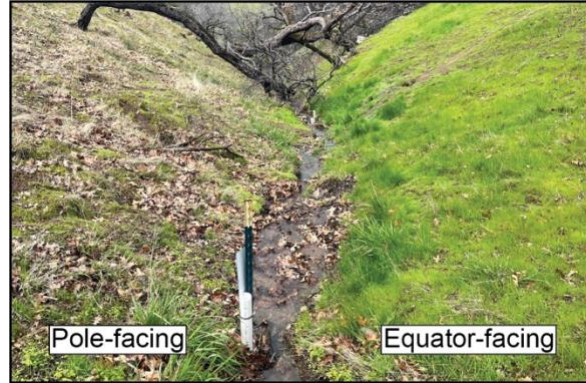
$$Flux \ [mmols/m2/s] \ = \frac{(slope \ x \frac{chamber \ volume}{chamber \ area})}{molecular \ weight \ of \ H_2O \ x \ 1000}$$

where the chamber volume was $0.125 \ m^3$, the surface area was $0.25 \ m^2$, and the molecular weight of H_2O was 18 g/mol.

We assumed the surface plot-scale estimates of water fluxes represent only grass transpiration but we acknowledge that these measurements also include evaporative fluxes. We believe this assumption is reasonable because transpiration has been shown to be the largest component of ET (Schlesinger & Jasechko, 2014). However, the reported grass transpiration measurements likely represent an upper bound or may overestimate grass transpiration due to variability in grass density (Supplementary Figure 2).

Supplementary Figure 1. Annotated image of the constructed chamber to measure grass transpiration within Arbor Creek Experimental Catchment.

Supplementary Figure 2. Image showing relatively higher grass density on the equator-facing slope compared to the pole-facing slope in March 2023.

1.2 Sapflow methods

Sap flux is known to vary radially through the sapwood but the radial profile is difficult to constrain. Here, we tested two possible radial flux profiles (1) constant sap flux across the sapwood based on the position with the maximum sap flux. The outer sapwood position typically had a much higher sap flux compared to the inner sap flux and was used to calculate volumetric sap flow (except T06 and T05). T06 had relatively similar sap flux between the inner and outer positions; therefore the outer position was used for the calculation for consistency. T05 had a higher inner position sap flux which was attributed to probe installation error. Specifically, the sap flow sensor may not have been installed deep enough beyond the bark. (2) Average sap flux between the outer and inner position which represents a linear decline in sap flux from the outer to inner position.

There are several limitations and assumptions made in converting heat-pulse measurements to hillslope-scale ET. Previous studies have noted that sap flow measurements can underestimate tree transpiration by as much as 35% (Steppe et al., 2010). Underestimates of transpiration may be due to wounding effects from sensor installation or probe misplacement in less functional xylem within the ring-prous oaks (Burgess et al., 2001; Burns et al., 2023; Miller, 1980) In addition, we had variable data coverage in April due to sensor installation, therefore the calculations of total tree sapflow begin on the earliest date with uniform data coverage (May 1st) which also contributes to an underestimate of total transpiration. By including two types of calculations, one based on the maximum sap flux and another based on the average sap flux, we provide a possible range of sap flow.

Table S1. Study tree characteristics			
Tree ID	DBH (cm)	Species	Sapwood thickness (cm)
T30	30.6	blue oak	4.9
T06	36.3	valley oak	6.6
T05	38.5	black oak	3.5
T26	42.5	black oak	4.5
T19	60.2	black oak	4.8
TBB	84.1	blue oak	5.8
TGPA	108.3	blue oak	5.8

Table S2. Hillslope-scale tree survey characteristics

Tree count	Species	DBH (cm)	Tree count (cont.)	Species (cont.)	DBH (cm, cont.)
1	blue oak	99.57	57	black oak	30.73
2	black oak	59.69	58	black oak	42.42
3	black oak	118.11	59	black oak	25.15
4	black oak	90.93	60	black oak	26.42
5	black oak	82.55	61	black oak	32.77
6	black oak	74.93	62	black oak	37.85
7	blue oak	42.42	63	black oak	33.02
8	blue oak	36.32	64	black oak	33.53
9	blue oak	44.70	65	black oak	33.78
10	blue oak	39.12	66	black oak	43.18
11	valley oak	138.18	67	black oak	61.21
12	black oak	49.53	68	black oak	35.56
13	black oak	72.14	69	black oak	44.20
14	black oak	68.58	70	blue oak	16.51
15	blue oak	46.99	71	blue oak	14.73
16	blue oak	46.74	72	blue oak	55.12
17	blue oak	54.61	73	blue oak	47.75
18	blue oak	30.48	74	blue oak	34.80
19	blue oak	63.50	75	blue oak	61.47
20	blue oak	29.21	76	blue oak	44.96
21	blue oak	60.71	77	blue oak	31.75
22	blue oak	60.20	78	blue oak	17.78
23	blue oak	50.55	79	blue oak	63.25
24	blue oak	76.96	80	blue oak	46.99
25	blue oak	68.33	81	blue oak	30.48
26	black oak	63.50	82	black oak	96.52
27	black oak	30.48	83	black oak	49.28
28	blue oak	52.58	84	black oak	61.21
29	blue oak	74.17	85	black oak	57.66
30	blue oak	50.55	86	black oak	46.23
31	blue oak	17.78	87	black oak	46.99
32	blue oak	19.05	88	black oak	35.56
33	blue oak	57.15	89	black oak	52.58
34	blue oak	109.22	90	black oak	83.06
35	blue oak	83.82	91	black oak	46.23
36	blue oak	79.25	92	black oak	56.39
37	black oak	43.18	93	black oak	33.78
38	black oak	26.16	94	blue oak	46.48
39	black oak	46.74	95	black oak	96.27
40	blue oak	53.34	96	black oak	63.25
41	black oak	50.04	97	blue oak	39.12
42	black oak	38.10	98	black oak	38.86
43	black oak	45.72	99	black oak	34.29
44	black oak	59.44	100	black oak	36.83
45	black oak	28.70	101	black oak	43.94
46	black oak	29.21	102	black oak	32.77
47	black oak	30.23	103	black oak	34.04
48	black oak	27.43	104	black oak	45.47
49	black oak	23.62	105	black oak	46.99
50	black oak	28.70	106	black oak	26.42
51	black oak	41.66	107	black oak	76.71
52	black oak	43.94	108	black oak	37.59
53	blue oak	31.75	109	black oak	49.78
54	blue oak	59.69	110	black oak	37.34
55	valley oak	36.32	111	black oak	49.28
56	black oak	31.75	112	black oak	44.96
			113	black oak	43.94

1.3 Open ET methods

The OpenET ensemble model includes five satellite-derived ET model inputs after the removal of outlier values (FAO, 2023). It should be noted that the SIMS model in OpenET (which is the only model that explicitly includes measurements of plant phenology through NDVI) is only developed for croplands, so it was not available within the OpenET ensemble for Arbor Creek Experimental Catchment (Volk et al., 2024). A detailed comparison of the differences, limitations and benefits of each model is outlined in literature developed by the Food and Agriculture Organization (FOA, 2023). Here, we provide a brief overview of model approaches.

Within the OpenET framework there are three ET models included based on a surface energy balance approach: geeSEBAL (Surface Energy Balance Algorithm for Land developed within the GEE environment; (Laipelt et al., 2021) DisALEXI (The Disaggregated Atmosphere – Land Exchange Inverse (Anderson et al., 2018) and eeMETRIC (Mapping ET at high Resolution with Internalized Calibration; (Allen Richard G. et al., 2007). The surface energy balance approach derives ET indirectly from the components of net radiation including the soil heat flux, latent heat flux and sensible heat flux.

In addition, there is one ET model based on the psychrometric approach, SSEBop (The Operational Simplified Surface Energy Balance; (Senay et al., 2017), and one model based on the Priestley-Taylor approach, PT_JPL (The Priestley – Taylor ET (Fisher et al., 2008). The psychrometric approach differs from the surface energy balance approach in that it does not solve for all components of the energy balance such as the sensible and soil heat flux. Instead this method uses a psychrometric constant for the air derived for the location and day of year that is adapted as a "surface" psychrometric constant (FOA, 2023). Lastly, the Preistley-Taylor approach determines actual ET from two primary components: setting an upper boundary of the ET flux and a set of eco-physiological constraining functions, reducing potential ET to actual ET (FOA, 2023).

2.0 Supporting materials results
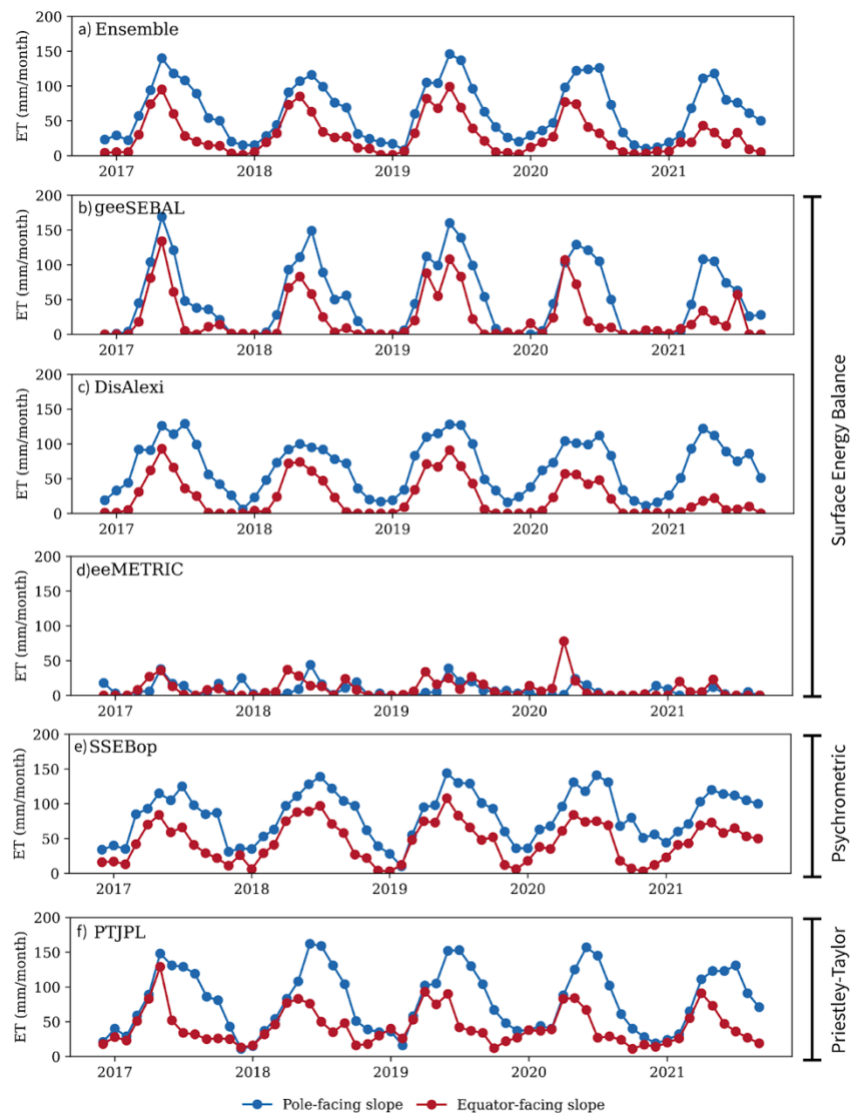**2.1 Sapflow results**

As expected, the total individual tree sap flow was lower when calculated based on the average sap flux compared to the assumed constant maximum sap flux across the sapwood (Supplementary Table 3). Therefore, the total hillslope-scale oak transpiration was 124 mm (average sap flux method) compared to 172 mm (maximum sap flux method). However, regardless of method, the relationship between DBH and total tree sap flow and the main conclusion of higher total ET on the pole-facing slope compared to the equator-facing slope remained true.

Table S3. Comparison of tree total sapflow between calculation methods

Tree ID	Total Average Sapflow (L)	Total Maximum Sapflow (L)
T05	3515	4273
T06	13728	13433
T19	9410	12988
T26	2935	5078
T30	864	1427
TGPA	13728	147387
TBB	97461	57962

2.2 Open ET results

Across all models (excluding eeMetric) the pole-facing slope has higher ET than the equator-facing slope (Supplementary Figure 3). Based on the timing and magnitude of ET reported by the eeMetric ET model, it is likely not accurate within Arbor Creek Experimental Catchment, may be flagged as an outlier within the filtering process and excluded from the Ensemble ET model calculation. However, at this time it is not possible to systematically extract which models are included within the Ensemble ET model with the OpenET API (Pers. Comm. Open ET developer team).

Supplementary Figure 3. Remotely-sensed monthly ET from the OpenET based a) Ensemble model, b) geeSEBAL model, c) DisAlexi model, d) eeMETRIC model, e) SSEBop model, and f) PTJPL model.

3.0 Supplementary material references

Allen Richard G., Tasumi Masahiro, & Trezza Ricardo. (2007). Satellite-Based Energy Balance for

Mapping Evapotranspiration with Internalized Calibration (METRIC)—Model. *Journal of*

Irrigation and Drainage Engineering, *133*(4), 380–394.

Anderson, M., Gao, F., Knipper, K., Hain, C., Dulaney, W., Baldocchi, D., Eichelmann, E., Hemes,

K., Yang, Y., Medellin-Azuara, J., & Kustas, W. (2018). Field-Scale Assessment of Land and

Water Use Change over the California Delta Using Remote Sensing. *Remote Sensing*, *10*(6), 889.

Burgess, S. S., Adams, M. A., Turner, N. C., Beverly, C. R., Ong, C. K., Khan, A. A., & Bleby, T. M.

(2001). An improved heat pulse method to measure low and reverse rates of sap flow in woody

plants. *Tree Physiology*, *21*(9), 589–598.

Burns, E. F., Rempe, D. M., Parsekian, A. D., Schmidt, L. M., Singha, K., & Barnard, H. R. (2023).

Ecohydrologic dynamics of rock moisture in a Montane catchment of the Colorado front range.

Water Resources Research, *59*(6). https://doi.org/10.1029/2022wr034117

FAO. (2023). *Remote sensing determination of evapotranspiration – Algorithms, strengths,*

weaknesses, uncertainty and best fit-for-purpose. FAO. https://doi.org/10.4060/cc8150en

Fisher, J. B., Tu, K. P., & Baldocchi, D. D. (2008). Global estimates of the land–atmosphere water

flux based on monthly AVHRR and ISLSCP-II data, validated at 16 FLUXNET sites. *Remote*

Sensing of Environment, *112*(3), 901–919.

Huxman, T. E., Cable, J. M., Ignace, D. D., Eilts, J. A., English, N. B., Weltzin, J., & Williams, D. G.

(2004). Response of net ecosystem gas exchange to a simulated precipitation pulse in a semi-arid

grassland: the role of native versus non-native grasses and soil texture. *Oecologia*, *141*(2), 295–

305.

Laipelt, L., Henrique Bloedow Kayser, R., Santos Fleischmann, A., Ruhoff, A., Bastiaanssen, W.,

Erickson, T. A., & Melton, F. (2021). Long-term monitoring of evapotranspiration using the

SEBAL algorithm and Google Earth Engine cloud computing. *ISPRS Journal of Photogrammetry*

and Remote Sensing: Official Publication of the International Society for Photogrammetry and Remote Sensing , *178*, 81–96.

Miller, D. H. (1980). *Measurement of Sap Flow and Transpiration in Ring-porous Oaks Using a Heat Pulse Velocity Technique*.

Schlesinger, W. H., & Jasechko, S. (2014). Transpiration in the global water cycle. *Agricultural and Forest Meteorology*, *189-190*, 115–117.

Senay, G. B., Schauer, M., Friedrichs, M., Velpuri, N. M., & Singh, R. K. (2017). Satellite-based water use dynamics using historical Landsat data (1984–2014) in the southwestern United States. *Remote Sensing of Environment*, *202*, 98–112.

Steppe, K., De Pauw, D. J. W., Doody, T. M., & Teskey, R. O. (2010). A comparison of sap flux density using thermal dissipation, heat pulse velocity and heat field deformation methods. *Agricultural and Forest Meteorology*, *150*(7), 1046–1056.

Volk, J. M., Huntington, J. L., Melton, F. S., Allen, R., Anderson, M., Fisher, J. B., Kilic, A., Ruhoff, A., Senay, G. B., Minor, B., Morton, C., Ott, T., Johnson, L., Comini de Andrade, B., Carrara, W., Doherty, C. T., Dunkerly, C., Friedrichs, M., Guzman, A., … Yang, Y. (2024). Assessing the accuracy of OpenET satellite-based evapotranspiration data to support water resource and land management applications. *Nature Water*, 1–13.